

## A conservative sequential fully implicit method for compositional reservoir simulation

Lee, S. H.; Tene, M.; Du, S.; Wen, X.; Efendiev, Y.

**DOI**

[10.1016/j.jcp.2020.109961](https://doi.org/10.1016/j.jcp.2020.109961)

**Publication date**

2021

**Document Version**

Final published version

**Published in**

Journal of Computational Physics

**Citation (APA)**

Lee, S. H., Tene, M., Du, S., Wen, X., & Efendiev, Y. (2021). A conservative sequential fully implicit method for compositional reservoir simulation. *Journal of Computational Physics*, 428, Article 109961. <https://doi.org/10.1016/j.jcp.2020.109961>

**Important note**

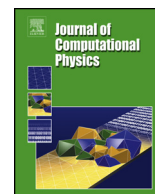
To cite this publication, please use the final published version (if applicable). Please check the document version above.

**Copyright**

Other than for strictly personal use, it is not permitted to download, forward or distribute the text or part of it, without the consent of the author(s) and/or copyright holder(s), unless the work is under an open content license such as Creative Commons.

**Takedown policy**

Please contact us and provide details if you believe this document breaches copyrights. We will remove access to the work immediately and investigate your claim.



# A conservative sequential fully implicit method for compositional reservoir simulation



S.H. Lee <sup>a,\*</sup>, M. Tene <sup>b,d</sup>, S. Du <sup>a</sup>, X. Wen <sup>a</sup>, Y. Efendiev <sup>c</sup>

<sup>a</sup> Chevron Energy Technology Co., 1500 Louisiana St., Houston, TX 77002, USA

<sup>b</sup> Dept. of Civil Engineering and Geosciences, Delft University of Technology, Delft, the Netherlands

<sup>c</sup> Dept. of Mathematics, Texas A&M, College Station, TX 77843-3368, USA

<sup>d</sup> Schlumberger Abingdon Tech. Center, Abingdon, OX14 4RU, UK

## ARTICLE INFO

### Article history:

Received 21 April 2020

Received in revised form 25 October 2020

Accepted 26 October 2020

Available online 1 November 2020

### Keywords:

Compositional reservoir simulation

Sequential fully implicit method

Phase equilibrium

Mass and volume conservation

Multi-phase flow

Porous media

## ABSTRACT

A conservative sequential fully implicit method is derived for compositional reservoir simulation. Multi-phase flow in porous media comprises coupled complex processes: i.e. elliptic flow equation, hyperbolic transport equation and highly nonlinear phase equilibrium equation. These processes contain very different mathematical characteristics that cannot be efficiently solved by one numerical method. As a result, the fully implicit method may become numerically complex and inefficient because the Jacobian includes the derivatives w.r.t. the variables from all of the different processes involved.

Jenny et al. (2004) [12] and Lee et al. (2015) [20] demonstrated that flow (pressure) and transport (saturation) for multi-phase flow without compositional effect can be efficiently solved by a sequential fully implicit method. However, the characteristics of the phase equilibrium equations are very different from those of the transport equations. This paper proposes an iterative method that solves the flow, transport and phase equilibrium equations in a sequential manner. The transport of hydrocarbons through porous media is governed by the multi-phase Darcy's equation, which is used to compute the phase velocities. The hydrocarbon components belonging to the same phase are transported with the same phase velocity. Upon arrival in the destination grid cell, these components are redistributed via a phase equilibrium calculation. This observation leads to simplification of the governing equations by reducing primary variables to four (i.e., pressure and three phase saturations). The nonlinear solution scheme composed of the stages outlined above is proven to preserve mass conservation, while a new degree of freedom, "thermodynamic flux", is introduced to ensure volume conservation. The sequential algorithm is solved iteratively until pressure, saturation, and phase composition are fully converged.

It is well-known that sequential solution schemes may require many iterations or fail to converge if the phase equilibrium calculation involves phase transition with a large volume change. This indicates that the current governing equations may not adequately describe fluid flux during rapid phase transition. With numerical examples we demonstrate that such numerical difficulties are successfully resolved via the thermodynamic flux term.

© 2020 Elsevier Inc. All rights reserved.

\* Corresponding author.

E-mail addresses: seonghl@gmail.com (S.H. Lee), matei.tene@slb.com (M. Tene), duvs@chevron.com (S. Du), xwen@chevron.com (X. Wen), efendiev@math.tamu.edu (Y. Efendiev).

<https://doi.org/10.1016/j.jcp.2020.109961>

0021-9991/© 2020 Elsevier Inc. All rights reserved.

## 1. Introduction

Complex physical processes in porous media (e.g. gas injection, miscible flooding, enhanced oil recovery, thermal recovery of heavy oil, etc.) can be effectively modeled by compositional reservoir simulation. Commercial reservoir simulators commonly adapt the governing equations in compositional formulation. This makes numerical simulation of compositional reservoir models an important practical tool in the management and production optimization of hydrocarbon reservoirs.

Commercial simulators usually employ an Equation of State (EoS) to calculate phase equilibrium. The equations of state, however, are highly nonlinear [35,34] and the convergence of numerical schemes designed to solve them is strongly dependent on the initial guess of the equilibrium factors (the ratio of gas and liquid mole fractions for each component) [24]. The cubic EoS, e.g. Peng-Robinson and Soave-Redlich-Kwong, often yields a trivial or non-convergent solution near a critical point or from an inaccurate initial guess. It used to be a challenge to identify the phase state, i.e., single or multi-phase, before Michelsen's [23] derivation of an important stability criterion that minimizes Gibbs free energy, thus, making the phase equilibrium calculation more stable and efficient. Many algorithms have been proposed in optimizing these calculations, e.g., successive substitution with a Newton method [25], reduced variables method [33], tie-line method [40], etc. The phase equilibrium with phase transition is, as a result, solved efficiently in commercial reservoir simulators.

Michelsen [25] proposed a generalized phase equilibrium calculation under various constraints for the thermodynamic state variables (e.g., isentropic, isenthalpic, and fixed volumetric flash computations). In the fully implicit compositional formulation with natural variables, the thermodynamic equilibrium condition is commonly included as an equality constraint of phase fugacities, while the total volume conservation is honored through the saturation constraint. All such algorithms require an accurate identification of phase state for numerical convergence. If a time-step involves phase transition, it becomes challenging to estimate accurate phase state and equilibrium constants. The nonlinear system of equations for primary variables is iteratively solved by a Newton method. In a sequential fully implicit formulation, the pressure and transport equations, coupled with thermodynamic equilibrium are solved in sequence [27,30]. Traditional sequential methods cannot exactly honor the volume or mass conservation. As a result, the fluid volume does not exactly satisfy the volume constraints, particularly in phase transition with a large volume change. This paper examines phase behavior in a confined space (porous media) that can be suitably used in compositional simulation. The flash calculation with fixed volume and temperature (VT-flash) is explored and compared with the traditional flash with fixed pressure and temperature (PT-flash). In addition, an unsteady "thermodynamic flux" is introduced to capture the effect of phase equilibrium in the pore space.

Many commercial reservoir models exhibit numerical instabilities during simulation that have not been fully understood and analyzed [46,42]. Even though the Fully Implicit Method (FIM) is numerically more dispersive than the Implicit Pressure and Explicit Saturation (IMPES) scheme, the former is widely used in practical applications because of its superior numerical stability. Unfortunately, since all the primary variables are coupled in FIM, it becomes increasingly difficult to extend conventional reservoir simulators to include new physics (surfactants, thermal effect, geomechanics, etc.). Furthermore, the complexity of mathematical structure, makes it challenging to analyze the numerical instability with such extensions.

The development of Multiscale Finite Volume Methods [11,12,21,22], has renewed interest in sequential fully implicit methods (SFI). A sequential algorithm can employ a modular programming design and provide natural physical interpretation [43]. Nevertheless, as the numerical stability becomes a daunting challenge for the complex multi-component fluid flow with nonlinear phase equilibrium computation, most commercial compositional simulators adapt FIM [3,45,4].

Lee et al. [20,18,19] and Hamon et al. [9,8,7] demonstrated numerical instability in multiphase flow often occurs due to discontinuities introduced by the conventional phase-potential based upwinding scheme. This simple fact was not obvious to simulation engineers and mathematicians for many years because of the complex structure of the fully-coupled large matrix system arising from the fully implicit formulation. In a sequential method, it becomes rather straightforward to examine numerical instabilities. Lee et al. [20] designed a hybrid upwinding scheme, which was shown to improve numerical stability significantly.

Recently Moncorgé et al. [27,28] and Møyner and Moncorgé [30] derived stable, convergent sequential fully implicit schemes for compositional multi-scale algorithms. Hajibeygi and Tchelepi [6] derived a compositional multiscale formulation based on overall composition, in which the phase equilibrium calculation was not included. Moncorgé et al. [27] employed the pressure equation based on total mass and divided the domain between FIM and SFI for a desired accuracy. In many cases, however, the subdomain allocated to FIM becomes dominant to make the algorithm expensive. Moncorgé et al. [28] also derived a two-step sequential method for compositional simulation: first, the pressure equation is constructed and solved, and then the solution of the coupled species transport equation follows. Later, Møyner and Moncorgé [30] derived another two-step sequential method for compositional simulation in which the whole system is first solved by a sequential method and then an additional post-processing of local transport iterations is applied in the non-convergent local domains. These researchers also found that the sequential algorithm cannot satisfy all the governing equations and constraints [28]. To mitigate the model inconsistency and numerical difficulties, the volume constraints needed to be relaxed. This clearly indicates an inconsistency in the governing equations for phase equilibrium and volume and mass conservation. This paper will examine this inconsistency closely and will introduce an additional degree of freedom to improve numerical convergence.

In the conventional compositional formulation, the transport equations are derived for each component, coupled with the phase equilibrium equation of state [1,45,4]. Instantaneous phase equilibrium is generally assumed. The number of independent variables becomes larger as the number of hydrocarbon components ( $N_c$ ) increases (i.e., Gibbs' phase rule:

$2 + N_c - N_p$ , where  $N_p$  represents the number of phases). This also makes the optimal selection of primary and secondary variables complex and system-dependent [41]. This paper leverages the simple physical observation that all the components in a phase move with the same phase velocity. Consequently, a multi-component system can be described by one transport equation for each phase, rather than each component. Once the phase velocity is computed, its composition can be derived from the component balance for each cell. Thus, the phase saturation becomes a primary variable, while the mole fractions can be back-calculated from the velocities and compositions of the fluid streams passing through the interfaces of each grid cell. Furthermore, as in the black oil formulation [21], a linear combination of the transport equations yields the pressure equation. This leads to a sequential formulation, where pressure is solved first, followed by the computation of total velocity, which is fixed during transport computation to give the phase saturations. The phase velocity and saturation are used to determine the phase compositions. Thermodynamic equilibrium is finally imposed, where the flash calculation yields the new compositions and saturations for each phase. This process is iterated until pressure, saturations and compositions converge. Clearly this sequential algorithm is described in natural variables and it becomes a black oil formulation by simply replacing the phase equilibrium calculation with the solution gas formulation. More importantly, this new formulation allows us to interpret the complex physical processes through porous media in a simple and natural way.

The paper is organized as follows. In section 2, the governing equations for three-phase transport are described and manipulated to yield one pressure equation and three saturation equations. The saturation equations are formulated in terms of total velocity and fractional flow. The discretized formulation for the equations is also derived and it is shown that compositions can be straightforwardly calculated from the component balance equation. In section 3, phase equilibrium methods are reviewed and “thermodynamic flux” is introduced to resolve non-convergence issue related to phase transition. In section 4, the compositional sequential fully implicit method is formulated, while the mathematical structure of compositional simulation is examined in section 5. The new sequential algorithms are summarized in section 6. Numerical examples are presented in section 7. Finally, the concluding remarks and discussion on future research directions follow in section 8.

## 2. Governing equations and discretized formulation

The many variables in compositional formulation are normally categorized as primary and secondary variables. The primary variables are solved from the conservation equations, while the secondary ones are back-calculated afterwards. Each choice for this partition has a significant impact on the convergence rate of algorithm and the structure of the Jacobian matrix that is constructed in the Newton iterative method [41]. Since the flow and transport equations are governed by the extended Darcy's law for multi-phase flow, the natural variables (e.g. pressure and saturations) form an optimal choice as primary variables for transport calculation. Molar component fractions, on the other hand, are the optimal choice as primary variables for the phase equilibrium computation. The belief that the fully implicit method provides the most stable solution is strongly ingrained in the reservoir simulation community [41] and consequently, the same set of primary variables are chosen both for transport and phase equilibrium computations [4,45,32]. By examining the governing equations, however, it is immediately apparent that the characteristics of transport and phase equilibrium equations are so different that their implicit simultaneous solution does not constitute an optimal algorithm. In [13] and [20], a sequentially coupled algorithm for pressure and saturation can be solved efficiently by an under-relaxation scheme facilitated by a trust region and hybrid upwinding methods. They showed that the sequential fully implicit method makes construction of the Jacobian simple and compact.

In compositional simulation, it is commonly accepted that the phase equilibrium is attained instantaneously, solely dependent on state variables, pressure, temperature and the mole fractions of the hydrocarbon components. Furthermore, the equations of state are widely adapted to provide a consistent phase equilibrium calculation. As mentioned earlier, a single numerical method is likely inefficient to solve two coupled physical processes with different nonlinearity and characteristics. We thus need to develop an efficient sequential algorithm that can be optimized for each physical process.

Towards developing a sequential fully implicit method for compositional simulation, we employ an iterative method in which all the major stages of computation (e.g. pressure, saturation, component transport, and phase equilibrium) are solved sequentially. The algorithm, as a result, enables us to select pressure and saturations (4 variables) as primary variables. All the other variables (e.g., capillary pressure, phase compositions, etc.) become secondary, since they can be computed by correlations, simple algebraic relations and component balance equations. An equation of state (e.g., Peng-Robinson EoS) is solved at the end of iteration to update the new state variables in thermodynamic equilibrium. If the solution changes among the primary variables do not lie below a specified error tolerance, the sequential algorithm is iterated until fully converged.

The governing equations for three-phase flow in a heterogeneous domain are given by

$$\frac{\partial}{\partial t} (\phi \rho_w S_w) = \nabla \cdot (\rho_w \lambda_w \cdot (\nabla p_w + g \rho_w \nabla H)) - q_w, \quad (1)$$

$$\frac{\partial}{\partial t} (\phi \rho_o S_o) = \nabla \cdot (\rho_o \lambda_o \cdot (\nabla p_o + g \rho_o \nabla H)) - q_o + E_o, \quad (2)$$

$$\frac{\partial}{\partial t} (\phi \rho_g S_g) = \nabla \cdot (\rho_g \lambda_g \cdot (\nabla p_g + g \rho_g \nabla H)) - q_g + E_g, \quad (3)$$

in the domain  $\Omega$ , with boundary conditions on  $\partial\Omega$ . Here,  $\lambda_\alpha = \mathbf{k}k_{r,\alpha}/\mu_\alpha$  is the mobility of phase  $\alpha$ , where  $\alpha = w, o, g$  (i.e., water, oil and gas).  $S_\alpha$ ,  $k_{r,\alpha}$ ,  $\mu_\alpha$ , and  $\rho_\alpha$  denote, respectively, the saturation, relative permeability, viscosity, and density of phase  $\alpha$ . The tensor  $\mathbf{k}$  describes the permeability field, which is usually represented as a complex spatial multi-scale function that tends to be highly discontinuous in discrete representations. Porosity is denoted by  $\phi$ ,  $p_\alpha$  is phase pressure,  $g$  is gravitational acceleration, and  $H$  denotes reservoir height. In general,  $\mu_\alpha$ ,  $\rho_\alpha$ , and  $\phi$  are functions of pressure, while the relative permeabilities,  $k_{r,\alpha}$ , are strong functions of saturation. In the right-hand side of equations,  $q_\alpha$  denotes the source/sink due to well production and injection.

Note that the governing equations include two additional terms,  $E_o$  and  $E_g$ , that represent mass transfer between the hydrocarbon phases (oil and gas) as required to satisfy phase equilibrium. It is generally computed either by the equation of state or via correlations.

Saturations are constrained by:

$$S_w + S_o + S_g = 1. \quad (4)$$

The phase pressures are related to the reference pressure by capillary pressures:

$$p_\alpha = p_{ref} + p_{c,\alpha}. \quad (5)$$

The capillary pressures are often measured for oil-water and oil-gas systems. If  $p_w$  is chosen as the reference pressure, then

$$p_o = p_w + p_{c,ow}, \quad (6)$$

$$p_g = p_w + p_{c,gw} = p_w + p_{c,go} + p_{c,ow}. \quad (7)$$

The phase fluxes are given by Darcy's law,

$$u_\alpha = -\lambda_\alpha \cdot (\nabla p_\alpha + g\rho_\alpha \nabla H). \quad (8)$$

The mass conservation in phase equilibrium calculation entails

$$E_o + E_g = 0. \quad (9)$$

In the compositional formulation, the phase density is the mass averaged density of each phase:

$$\rho_o = \frac{\sum m_c x_c}{v_o}, \quad (10)$$

$$\rho_g = \frac{\sum m_c y_c}{v_g}. \quad (11)$$

Here,  $x_c$  and  $y_c$  denote the mole fraction of component  $c$  in oil and gas phases, respectively.  $v_o$  and  $v_g$  are the molar volumes for oil and gas phases and  $m_c$  is the molecular weight for component  $c$ . For simplicity, the phase equilibrium is only studied between the hydrocarbon phases. It is thus assumed that the system contains no water-soluble components. In addition,  $v_w$  denotes the molar volume of water.

If the mole fractions of water, oil and gas phases are given by  $M_w$ ,  $M_o$  and  $M_g$ , respectively, the phase saturations can be expressed as

$$S_w = \frac{M_w v_w}{V_t}, \quad S_o = \frac{M_o v_o}{V_t}, \quad \text{and} \quad S_g = \frac{M_g v_g}{V_t}, \quad (12)$$

where the molar volume of the multi-phase fluid,  $V_t$ , is given by

$$V_t = M_o v_o + M_g v_g + M_w v_w. \quad (13)$$

The discretized component balance equation for each cell can be derived as

$$\frac{V_p(M_o + M_g)}{\Delta t V_t} (z_c^{n+1} - z_c^n) = \nabla \cdot \left( \frac{u_o}{v_o} x_c + \frac{u_g}{v_g} y_c \right). \quad (14)$$

Here,  $\Delta t$  is the time step size, superscripts  $n$  and  $n+1$  denote the previous and current time levels, respectively.  $V_p$  is the pore volume and  $z_c$  is the total mole fraction for component  $c$ .

For given pressure, temperature and total fluid composition, the EoS (e.g., Peng-Robinson) yields the density, volume, and composition for each phase:

$$E : \{p, T, z_c\} \rightarrow \{L, x_c, y_c, \rho_o, \rho_g, v_o, v_g\}, \quad (15)$$

where  $L$  is the mole fraction of the oil phase.

For the numerical examples, the water phase pressure,  $p = p_w$ , is chosen as primary variable. The following semi-discrete form of the equations is obtained:

$$\frac{\phi^{n+1} \rho_w^{n+1} S_w^{n+1} - \phi^n \rho_w^n S_w^n}{\Delta t} = \nabla \cdot (\rho_w \lambda_w \cdot (\nabla p + g \rho_w \nabla H))^{n+1} - q_w^{n+1}, \quad (16)$$

$$\frac{\phi^{n+1} \rho_o^{n+1} S_o^{n+1} - \phi^n \rho_o^n S_o^n}{\Delta t} = \nabla \cdot (\rho_o \lambda_o \cdot (\nabla(p + p_{cow}) + g \rho_o \nabla H))^{n+1} - q_o^{n+1} + E_o^{n+1}, \quad (17)$$

$$\frac{\phi^{n+1} \rho_g^{n+1} S_g^{n+1} - \phi^n \rho_g^n S_g^n}{\Delta t} = \nabla \cdot (\rho_g \lambda_g \cdot (\nabla(p + p_{cgw}) + g \rho_g \nabla H))^{n+1} - q_g^{n+1} + E_g^{n+1}. \quad (18)$$

Multiplication of Eqs. (16) to (18) with

$$\omega_w = \frac{1}{\rho_w^{n+1}}, \quad \omega_o = \frac{1}{\rho_o^{n+1}}, \quad \text{and} \quad \omega_g = \frac{1}{\rho_g^{n+1}}, \quad (19)$$

respectively, and summation of the resulting equations yields

$$\frac{\phi^{n+1}}{\Delta t} - \frac{\phi^n}{\Delta t} \left( \sum_{\ell \in \{w, o, g\}} \omega_\ell^{n+1} \rho_\ell^n S_\ell^n \right) = R, \quad (20)$$

where  $R = \omega_w$ (rhs of Eq. (16)) +  $\omega_o$ (rhs of Eq. (17)) +  $\omega_g$ (rhs of Eq. (18)). Eq. (20) is the overall mass balance equation, in which saturations at the current time-level,  $n + 1$ , do not appear explicitly. To simplify the nonlinearities of parameters in the pressure equation, the coefficients in the convective terms (i.e.,  $\omega$ 's, mobilities, and formation volume factors on the right-hand side of Eq. (20)) are lagged by one Newton iteration. However, the pressure dependent coefficients in the accumulation term (e.g.,  $\phi^{n+1}$  and  $\omega^{n+1}$ ) as well as the source/sink terms ( $\omega^{n+1} q^{n+1}$ ) are linearized w.r.t. pressure. After rearrangement, the following equation is obtained:

$$C \frac{(p^{\nu+1} - p^\nu)}{\Delta t} - \omega_w \nabla \cdot (\lambda_w^\nu \cdot \nabla p^{\nu+1}) - \omega_o \nabla \cdot (\lambda_o^\nu \cdot \nabla p^{\nu+1}) - \omega_g \nabla \cdot (\lambda_g^\nu \cdot \nabla p^{\nu+1}) = RHS1, \quad (21)$$

with

$$C = \frac{\partial \phi}{\partial p} \Big|^\nu - \phi^n \left( \frac{\partial \omega_w}{\partial p} \Big|^\nu \rho_w^n S_w^n + \frac{\partial \omega_o}{\partial p} \Big|^\nu \rho_o^n S_o^n + \frac{\partial \omega_g}{\partial p} \Big|^\nu \rho_g^n S_g^n \right) + \Delta t \left( \frac{\partial \omega_w q_w}{\partial p} \Big|^\nu + \frac{\partial \omega_o q_o}{\partial p} \Big|^\nu + \frac{\partial \omega_g q_g}{\partial p} \Big|^\nu - \frac{\partial \omega_o E_o}{\partial p} \Big|^\nu - \frac{\partial \omega_g E_g}{\partial p} \Big|^\nu \right), \quad (22)$$

$$RHS1 = \frac{\phi^n}{\Delta t} (\omega_w \rho_w^n S_w^n + \omega_o \rho_o^n S_o^n + \omega_g \rho_g^n S_g^n) - \frac{\phi^\nu}{\Delta t} - (\omega_w q_w^\nu + \omega_o q_o^\nu + \omega_g q_g^\nu) + (\omega_o E_o^\nu + \omega_g E_g^\nu) + \omega_w \nabla \cdot (g \rho_w \lambda_w^\nu \cdot \nabla H) + \omega_o \nabla \cdot (g \rho_o \lambda_o^\nu \cdot \nabla H) + \omega_g \nabla \cdot (g \rho_g \lambda_g^\nu \cdot \nabla H) + \omega_o \nabla \cdot (\lambda_o^\nu \cdot \nabla p_{cow}) + \omega_g \nabla \cdot (\lambda_g^\nu \cdot \nabla p_{cgw}), \quad (23)$$

and

$$\lambda_o^\nu = \rho_o^\nu \lambda_o^\nu, \quad \lambda_w^\nu = \rho_w^\nu \lambda_w^\nu, \quad \text{and} \quad \lambda_g^\nu = \rho_g^\nu \lambda_g^\nu. \quad (24)$$

In these expressions,  $\nu$  and  $\nu + 1$  denote the previous and current Newton iteration levels, respectively.

Eq. (21) is solved iteratively for  $p^{\nu+1}$ , and the updated pressure is then used to derive the linearized transport equations:

$$\frac{\phi^{\nu+1} \rho_\alpha S_\alpha^{\nu+1} - \phi^\nu \rho_\alpha S_\alpha^\nu}{\Delta t} = \nabla \cdot \left[ \rho_\alpha^{\nu+1} (\lambda_\alpha^\nu + \sum_{\ell \in \{w, o, g\}} \frac{\partial \lambda_\alpha}{\partial S_\ell} \Big|^\nu (S_\ell^{\nu+1} - S_\ell^\nu)) \cdot (\nabla p^{\nu+1} + g \rho_\alpha^{\nu+1} \nabla H) \right] - (q_\alpha - E_\alpha) \Big|_{p^{\nu+1}} - \sum_{\ell \in \{w, o, g\}} \left( \frac{\partial q_\alpha}{\partial S_\ell} - \frac{\partial E_\alpha}{\partial S_\ell} \right) \Big|_{p^{\nu+1}, S^\nu} (S_\ell^{\nu+1} - S_\ell^\nu), \quad (25)$$

where  $\alpha \in \{w, o, g\}$ . In common practice, only two out of the three equations, Eq. (25), are solved; and the saturation of the third phase is obtained from Eq. (4). Møyner and Moncorgé [29] found that three saturation solutions from Eq. (25) yield better convergence by relaxing the volume constraint that the pore volume and fluid volume are equal in the iterative process. Note that the states at  $\nu$ ,  $\nu + 1$ , and  $n + 1$  are identical when the Newton-Raphson process is converged.

Eqs. (21) and (25) are solved for  $p^{v+1}$  and  $S_\alpha^{v+1}$ , respectively. In solving the saturation equations, we employ the fixed total velocity and fractional flow formulation [11,21], described in the following subsections 2.1 and 2.3. The density,  $\rho_\alpha^{v+1}$ , is updated using the new pressure while the other secondary variables,  $\{x_c^{v+1}\}$ ,  $\{y_c^{v+1}\}$ , and  $\{z_c^{v+1}\}$  will be straightforwardly computed from the component balance equation, as described in subsection 2.4. Using the phase equilibrium calculation, Eq. (15), the state variables are updated:

$$E : \{p^{v+1}, T, \{z_c^{v+1}\}\} \rightarrow \{\rho_\alpha^{\bullet,v+1}, \{x_c^{\bullet,v+1}\}, \{y_c^{\bullet,v+1}\}, v_\alpha^{\bullet,v+1}\}, \quad \text{where } \alpha \in \{w, o, g\}. \quad (26)$$

The superscript  $\bullet$  indicates a state variable in thermodynamic equilibrium. The updated variables in Eq. (26) readily yield the new saturations,  $S_\alpha^{\bullet,v+1}$ , which are consistent with EoS.

### 2.1. Conservative total velocity field

Equation (21) is solved with appropriate Dirichlet or Neumann boundary conditions, as dictated by the controls of the wells present in the reservoir. The resulting pressure solution is then used to compute locally conservative fine-scale phase velocities, which are necessary for accurate transport computations (i.e. solving the saturation equations);

$$u_T = u_w + u_o + u_g \\ = -\lambda_w \cdot \nabla(p + \rho_w gH) - \lambda_o \cdot \nabla(p + p_{cow} + \rho_o gH) - \lambda_g \cdot \nabla(p + p_{cgw} + \rho_g gH). \quad (27)$$

Trangenstein and Bell [38] observed that the pressure and saturation of incompressible flow are decoupled by fixing the total velocity,  $u_T$ , which is defined as the sum of the phase velocities. An ideal algorithm for incompressible flow is thus a numerical scheme that sequentially couples pressure and saturations with fixed total velocity. In this paper, the transport equations with total velocity and fractional flow formulation [14,21] are extended to compositional simulation.

### 2.2. Saturation solution

Using the conservative phase velocity field, Eq. (25) can be written as

$$\frac{\phi^{v+1} \rho_\alpha^{v+1} S_\alpha^{v+1} - \phi^n \rho_\alpha^n S_\alpha^n}{\Delta t} = \rho_\alpha^{v+1} \nabla \cdot \left( u_\alpha^{v+1} \left( 1 + \frac{1}{\lambda_\alpha^v} \sum_\ell \frac{\partial \lambda_\alpha}{\partial S_\ell} \Big|_v (S_\ell^{v+1} - S_\ell^v) \right) \right) \\ - \left( (q_\alpha - E_\alpha) \Big|_{p^{v+1}, S^v} + \sum_\ell \left( \frac{\partial q_\alpha}{\partial S_\ell} - \frac{\partial E_\alpha}{\partial S_\ell} \right) \Big|_{p^{v+1}, S^v} (S_\ell^{v+1} - S_\ell^v) \right). \quad (28)$$

The phase velocity in the right-hand side of Eq. (28) can be further expressed in terms of the total velocity and gravitational and capillary velocities:

$$u_\alpha^{v+1} = \frac{\lambda_\alpha}{\lambda_T} \left( u_T^{v+1} - \sum_\beta \lambda_\beta (\rho_\beta g - \rho_\alpha g) \nabla H - \sum_\beta \lambda_\beta (\nabla p_{c\beta w} - \nabla p_{c\alpha w}) \right), \quad (29)$$

where  $\lambda_T \equiv \sum \lambda_i$  and  $p_{c\beta w} = 0$  for  $\beta = w$ . With the total velocity fixed, Eqs. (28) and (29) are solved for saturations at the new iteration level,  $S_\alpha^{v+1}$ .

### 2.3. Fractional flow equations

The phase velocity in Eq. (29) can be rewritten in a concise form:

$$u_\alpha = f_\alpha^U(S) u_T + \sum_\beta f_{\alpha,\beta}^G(S) C_{\alpha,\beta}^G + \sum_\beta f_{\alpha,\beta}^C(S) C_{\alpha,\beta}^C. \quad (30)$$

The fractional-flow functions are derived as:

$$f_\alpha^U = \frac{\tilde{m}_\alpha k_{r\alpha}}{\sum_\ell \tilde{m}_\ell k_{r\ell}}, \quad (31)$$

$$f_{\alpha,\beta}^G = f_{\alpha,\beta}^C = \frac{\tilde{m}_\alpha \tilde{m}_\beta k_{r\alpha} k_{r\beta}}{\sum_\ell \tilde{m}_\ell k_{r\ell}}. \quad (32)$$

Here,  $\tilde{m}_\alpha (= \mu_w / \mu_\alpha)$  is the inverse viscosity ratio with respect to the viscosity of water phase. Note that  $\sum_\alpha f_\alpha^U = 1$ . The velocities due to buoyancy and capillary forces [20,18,19] are characterized by the following dimensionless gravity and capillary numbers, respectively:

$$C_{\alpha,\beta}^G = \frac{kg(\rho_\beta - \rho_\alpha)}{\mu_w u_c} \nabla H, \quad (33)$$

$$C_{\alpha,\beta}^C = \frac{k(\nabla p_c^\beta - \nabla p_c^\alpha)}{\mu_w u_c}, \quad (34)$$

where  $u_c$  is a characteristic velocity. Note that the velocities  $u_T$  and  $u_\alpha$  in Eq. (30) are normalized with respect to  $u_c$ . From here on, all the quantities are normalized w.r.t. characteristic variables,  $l_c$ ,  $u_c$ ,  $t_c (= l_c/u_c)$ , and  $p_c (= u_c l_c \mu_w/k)$ .

In a discretized model, the one-point upwinding scheme based on the phase velocity is commonly applied for fractional flow [2]. Lee et al. [20,18,19] observed that many numerical instabilities are caused by the flip-flopping of phase upwind direction. They proposed a hybrid upwinding method that greatly enhances numerical stability of multi-phase flow in the presence of gravity and capillary forces. Similar hybrid upwind schemes can be found in [9,7]. From Eqs. (30)–(34) it is apparent that the flux functions from gravity and capillary forces have a similar functional form: in the former the driving force is the difference of phase densities, while in the latter, that of capillary pressure gradients. Note that the fractional flows,  $f_{\alpha,\beta}^G$  and  $f_{\alpha,\beta}^C$  are identical in Eq. (32).

#### 2.4. Component balance equation

In the formulation presented in this paper, the phase mixing (component transfer between phases) is not involved in the solution of the saturation equations. This approximation renders the algorithm simple, allowing the separation of each process into a dedicated sequential step. The component balance equation, as a result, can be straightforwardly solved, given component compositions from the previous time-step and the phase velocities between cells. Note that all the components in a phase move with the same phase velocity between two neighboring cells. The mass fraction of components is solved from the component transport equation and then it will be converted into the mole fraction of components. The mass fraction of component  $c$  of phase  $\alpha$  in cell  $i$ , can be readily computed from the mole fraction:

$$\xi_{c,i}^\alpha = \frac{x_{c,i}^\alpha m_c}{\sum_\ell x_{\ell,i}^\alpha m_\ell}. \quad (35)$$

Here,  $x_{c,i}^\alpha$  and  $\xi_{c,i}^\alpha$  denote the mole fraction and mass fraction of component  $c$  in phase  $\alpha$  of cell  $i$ , respectively, and  $m_c$  is the molecular weight of component  $c$ .

The component balance equation for component  $c$  in cell  $i$  can thus be written as:

$$\frac{1}{\Delta t} (V_{\alpha,i}^{n+1} \rho_{\alpha,i}^{n+1} \xi_{c,i}^{\alpha,n+1} - V_{\alpha,i}^n \rho_{\alpha,i}^n \xi_{c,i}^{\alpha,n}) = \sum_{j \in \mathfrak{N}_i} \rho_{\alpha,ij}^{n+1} u_{\alpha,ij}^{n+1} \xi_{c,ij}^{\alpha,n+1}, \quad (36)$$

where  $j \in \mathfrak{N}_i$  denotes the neighboring cells connected to cell  $i$  and the subscript  $ij$  indicates the properties at the cell interface of  $i$  and  $j$ .  $V_{\alpha,i}$  is the  $\alpha$ -phase volume in cell  $i$ . As in the conventional upwinding method, the mole fraction of component  $c$  at the cell interface is determined by the phase velocity at the interface:

$$\begin{aligned} x_{c,ij}^{\alpha,n+1} &= x_{c,i}^{\alpha,n+1}, & \text{if } u_{\alpha,ij}^{n+1} \geq 0, \\ &= x_{c,j}^{\alpha,n+1}, & \text{if } u_{\alpha,ij}^{n+1} < 0. \end{aligned} \quad (37)$$

The phase density  $\rho_{\alpha,ij}^{n+1}$  at the cell interface can be similarly specified as a one-point upwind value. Note that for given phase velocities between cells, the system of linear equations, Eq. (36), can be directly solved. The mass fraction can be converted to the mole fraction:

$$x_{c,i}^\alpha = \frac{\xi_{c,i}^\alpha / m_c}{\sum_\ell \xi_{\ell,i}^\alpha / m_\ell}. \quad (38)$$

### 3. Phase equilibrium calculation

The phase equilibrium calculation of hydrocarbons is highly non-linear and entails special algorithms to ensure numerical convergence [23,24]. The equation of state is a cubic equation with two parameters that can only converge with good initial estimates of the equilibrium factors. Before the pioneering work of Michelsen [23], it was challenging to identify the number of stable phases. Since a reservoir simulation includes many phase equilibrium computations, it is crucial to optimize the algorithm to be numerically efficient and robust. In commercial reservoir simulation, the Peng-Robinson Equation of State (PREoS) [35] is exclusively used. The numerical examples presented in this paper also use PREoS for phase equilibrium calculation.

In compositional simulation, it is often assumed that phase equilibrium is attained instantaneously for given pressure and temperature (PT-flash) in a finite volume cell [4,45]. This commonly accepted assumption is not rigorous or accurate due to incomplete mixing in a heterogeneous grid block and the large scale of grids [37]. There have been several studies

to address this non-equilibrium phase behavior [10,31,36]. It is apparent that phase equilibrium in porous media cannot be described by a simple fugacity equality with given pressure and temperature. It involves ambiguity and complexity due to the non-equilibrium thermodynamics, the diffusion process between phases, pore volume constraint, scale difference in pores and simulation grids, etc. Especially, if the pores are small (e.g., nano pores), other physical phenomena play an important role in the thermodynamics equilibrium [5].

Clearly the equilibrium condition of PT-flash is not suited for fluid in porous media because of the strong pore volume constraint, which may be violated if the phase equilibrium calculation induces a large fluid volume change. It is thus important to explore different flash calculations based on state functions. For instance, the phase equilibrium computation with specified volume and temperature (VT-flash) may provide a more relevant condition in porous media. The flash calculation algorithm for PT and VT flashes is described next and a modified PT-flash with a volume constraint, obtained by adjusting fluid densities, is also proposed. The modified PT-flash entails a simpler computation than the VT-flash and conserves the volume during phase transition. As the phase equilibrium is a volumetrically averaged variable with large uncertainties and complexity, it can be a practical alternative that is simple to compute and also provides the conservation of mass and volume.

This modified version of PT-flash is designed to conserve the total fluid volume by compressing or expanding the gas volume. As discussed before, a sudden volume change in phase transition creates numerical difficulties in compositional simulation. In a constant composition expansion, the liquid volume monotonically increases as pressure decreases, but the total fluid volume increases quickly as the gas comes out when the pressure drops below the bubble point. Even though the mass in the gas phase is small, the gas volume is so disproportionately large that the sum of saturations becomes bigger than one. This cannot be modeled easily by the current multi-phase Darcy's equation. To address this, either an infinitesimally small time-step size needs to be employed, with which the multi-phase Darcy's equation is asymptotically still valid, or an intermediate stage is required to conserve mass/volume. The latter can be achieved via a simple modification of the phase equilibrium that allows a transient gas phase to honor total volume and mass of hydrocarbons. The phase split is still based on PT-flash.

Finally, we introduce a new degree of freedom, "thermodynamic flux", that allows an additional fluid flux to satisfy the volume constraint. In porous media, a fluid cannot achieve phase equilibrium instantaneously at given pressure and temperature. The extra volume (positive or negative) needs a relaxation time to dissipate through the neighboring cells. This extra flux is physically induced by the volume change from phase equilibrium. This new concept is carefully examined in this section.

### 3.1. PT-Flash

There are two major algorithms to solve the equation of state: (1) Direct successive substitution and (2) Newton's method for linearized equations. To expedite computation, Michelsen [25] also proposed a mixed strategy of successive substitution and Newton's method.

#### Successive Substitution

The initial guess of the equilibrium constant for component  $c$  is generally provided by Wilson's equation:

$$\ln K_c^0 = \ln \frac{p_c^c}{p} + 5.373(1 + \omega^c) \left( 1 - \frac{T_c^c}{T} \right). \quad (39)$$

Here,  $T_c^c$ ,  $p_c^c$ , and  $\omega^c$  are the critical temperature, critical pressure, and acentric factor for component  $c$ , respectively. From the initial guess of the equilibrium constants, the fugacity can be computed as shown in [35]. The equilibrium constant is iteratively updated to convergence:

$$K_c^{v+1} = \frac{f_c^{o,v}(p, T, \{x_i\})}{f_c^{g,v}(p, T, \{y_i\})}. \quad (40)$$

#### Newton Method

The set of equations to solve for phase equilibrium is

$$f_c(K) = \left( \ln(v_c/M_g) + \ln \phi_c^V \right) - \left( \ln(l_c/M_o) + \ln \phi_c^L \right) = 0, \quad (41)$$

where  $v_c$  and  $l_c$  are the number of moles of component  $c$  in the gas and oil phases for one mole of the gas and oil mixture, respectively.  $M_g$  and  $M_o$  denote the mole fractions of the gas and oil phases, and  $\phi_c^V$  and  $\phi_c^L$  are the fugacity coefficients for component  $c$  in gas and oil. Eq. (41) can be iteratively solved by a Newton-Raphson method [24].

### 3.2. VT-Flash

#### Nested Minimization

The VT-flash can be straightforwardly implemented by applying a nested minimization method with an inner loop of PT-flash. The outer loop will find the pressure which satisfies constant volume [25,26]. As PT-flash is well established, this nested method can be easily implemented and is robust; however, it may not be computationally efficient.

### Newton Method

An efficient computation of phase equilibrium can be obtained by a Newton-Raphson method [25].

$$\begin{pmatrix} M_{ij} & g_p \\ g_p^T & E_{pp} \end{pmatrix} + \begin{pmatrix} \Delta V \\ \Delta \ln p \end{pmatrix} + \begin{pmatrix} g \\ r_p \end{pmatrix} = 0, \quad (42)$$

where

$$g_i = \ln y_i + \ln \phi_i(y, T, p) - \ln x_i - \ln \phi_i(x, T, p), \quad (43)$$

$$M_{ij} = \frac{\partial g_i}{\partial v_j}, \quad (44)$$

$$g_{p,i} = p \left( \frac{\partial \ln \phi_i(y, T, p)}{\partial p} - \frac{\partial \ln \phi_i(x, T, p)}{\partial p} \right), \text{ for } i = 1, N_c, \quad (45)$$

$$E_{pp} = \frac{p^2}{RT} \frac{\partial V}{\partial p}. \quad (46)$$

### 3.3. Modified PT-Flash

Considering the ambiguity and uncertainty associated with phase equilibrium in porous media, a modified PT phase equilibrium is proposed. It honors volume and mass conservation, by modifying the fluid density computation to conserve volume. The main advantage of this modified phase equilibrium lies in the reduction of numerical instabilities due to the sudden increase of the total volume during phase transition.

From the constant composition expansion, the liquid density does not change much as pressure decreases, but the gas density is much more sensitive to pressure change. Furthermore, the first small amount of gas coming out from the fluid is likely entrapped in pores by the capillary pressure. It is thus a reasonable assumption that gas may have a different pressure from oil. As a result, if the volumes and densities of gas and oil are given by PT-flash as  $V_g, V_o, \rho_o$ , and  $\rho_g$ , respectively, the meta-stable gas volume and density can be employed:

$$V_g^* = V_0 - V_o, \quad (47)$$

$$\rho_g^* = \rho_g \frac{V_g}{V_g^*}. \quad (48)$$

Here,  $V_0$  is the total hydrocarbon volume before the flash calculation. For the case with no gas phase (near a dew point) after the flash calculation, the oil density can be adjusted to satisfy the volume constraint:

$$V_o^* = V_0, \quad (49)$$

$$\rho_o^* = \rho_o \frac{V_o}{V_o^*}. \quad (50)$$

### 3.4. Thermodynamic flux

The VT-flash entails an additional degree of freedom, thermodynamic pressure,  $p^{thm}$ , to satisfy the volume constraint, whereas the dynamic pressure,  $p^{dyn}$ , from the transport equation is employed in PT-flash, without strictly honoring the volume constraint. If the total volume does not change much in phase equilibrium calculation,  $p^{thm} \sim p^{dyn}$ . In phase transition, these two pressures can be substantially different. Clearly the conventional governing equations may not accurately describe the transient phenomena. It is important to understand the actual physical path that a fluid may follow in reaching a phase equilibrium in porous media.

If VT-flash is applied, the transport equation becomes easy to solve without volume balance error, but a noticeable discrepancy between thermodynamic and dynamic pressures remains. An additional model to describe the flux due to the non-equilibrium pressure ( $= p^{thm} - p^{dyn}$ ) is needed. We propose that a thermodynamic flux between two adjacent cells  $i$  and  $j$  is proportional to the difference of non-equilibrium pressures:

$$q_{ij}^{thm} = T_{ij}(p_i^{thm} - p_i^{dyn} - p_j^{thm} + p_j^{dyn}). \quad (51)$$

This additional flux will reduce the difference of the two pressures to reach a true phase equilibrium. Nonetheless, solving Eq. (51) can be expensive as it may require a global solution. Moncorgé et al. [28] and Møyner and Moncorgé [29] noted that the phase transition domain is very localized and it does not affect the global solution significantly. It mainly impacts the local convergence around the phase transition domain.

In this paper, instead of solving Eq. (51) rigorously, a simple approximation to estimate the thermodynamic flux is derived by computing the difference between fluid volume and pore volume. A fluid volume increase accompanied in phase

transition from a sole liquid phase to the two phase regime (oil and gas), the extra fluid volume is allowed to move out of the host cell to the downstream cell (or toward the production well). In the case of fluid volume shrinkage, often encountered in miscible flooding, the neighboring fluid enters the cell to fill the void created by the phase transition. With this mechanism in place, the sequential algorithm is iterated to achieve numerical convergence. This simple approximation algorithm is used for the numerical examples in section 7.

#### 4. Sequential fully implicit scheme

Since the transport equation of multi-phase flow and phase equilibrium equations are derived for distinctly different processes, it is desirable to develop a sequential algorithm that employs a modular programming design and provides natural interpretation of physical process [43].

Ács et al. [1] derived a direct sequential IMPES method, and Watts [43] derived an implicit sequential method to improve numerical convergence and stability over the IMPES method. Nevertheless, the numerical stability is a daunting challenge for the complex multi-component fluid flow with nonlinear phase equilibrium computation, and, as a result, the industry mostly adapts the Fully Implicit Method in commercial compositional simulators [3,45,4].

Recently stable and convergent sequential fully implicit schemes were actively investigated [28,27,30]. Developers of SFI algorithms for compositional simulation noted that it was not possible to derive an algorithm that exactly satisfies the governing equations and constraints [28]. Some inconsistencies are tolerated to provide a convergent solution within an acceptable error tolerance. This might indicate that the pressure, saturation, and phase behavior are strongly coupled and, as a result, the sequential algorithm may not model correctly strongly coupled terms. It was noted that the numerical inconsistencies are localized around a domain where a large volume change occurs due to phase transition. This observation, however, may also indicate that the governing equation may not accurately describe the process in which the total fluid volume is significantly different from the pore volume. It may violate the fundamental assumption of Darcy's equation for multi-phase flow. Simulators often adapt rescaling or chopping variables that lie outside of the physical boundary. The mathematical implication of rescaling or chopping variables in such highly nonlinear problems is not fully understood. It is quite possible that the fully implicit algorithm may allow a solution that is not consistent or convergent for a highly nonlinear, coupled problem. To shed light on these difficult nonlinearity issues, the consistency and convergence of the fully implicit scheme will be examined in a forthcoming paper.

##### 4.1. Reordering saturation equations

It is well-known that the convergence of hyperbolic saturation equations can be improved significantly if the variables are reordered, based on their potential values [17] or upwind directions [16]. Let  $P$  be the permutation matrix that reorders cells from natural order to upwind-direction based order. The linearized saturation equation, Eq. (28), is first expressed in a compact matrix form:

$$AS = R \tag{52}$$

where  $S$  is the saturation vector  $[S_w^{\nu+1}, S_o^{\nu+1}, S_g^{\nu+1}]^T$  and  $R$  is the right-hand side vector. Applying the permutation matrix  $P$ , Eq. (52) is reordered as

$$\tilde{A}\tilde{S} = \tilde{R}, \tag{53}$$

where

$$\tilde{A} = PAP^T, \quad \tilde{S} = PS, \quad \text{and} \quad \tilde{R} = PR.$$

Note that the permutation matrix is orthogonal ( $PP^T = I$ ). When the fluid properties at the upwind location change substantially during the phase equilibrium calculation, the reordering scheme can be employed to improve numerical convergence. The phase equilibrium operator  $E$  will yield

$$\{S_o^{\bullet,\nu}, S_g^{\bullet,\nu}, x_j^{\bullet,\nu}, y_j^{\bullet,\nu}, \rho_o^{\bullet,\nu}, \rho_g^{\bullet,\nu}, \mu_o^{\bullet,\nu}, \mu_g^{\bullet,\nu}\} = E(\{S_o^{\nu}, S_g^{\nu}, x_j^{\nu}, y_j^{\nu}, \rho_o^{\nu}, \rho_g^{\nu}, \mu_o^{\nu}, \mu_g^{\nu}\}). \tag{54}$$

In the reordered saturation equation, Eq. (53), cell saturation and phase equilibrium are sequentially combined for each cell. They are evaluated in a cell-by-cell basis. This reordered scheme will improve the saturation convergence, especially when phase equilibrium significantly alters cell properties (e.g., saturation, phase density, viscosity, etc.).

#### 5. Mathematical structure

The phase equilibrium calculation is very nonlinear and numerical convergence is assured only if the initial estimate is close to the final solution. In general, the multi-phase flow is assumed to attain instantaneous phase equilibrium, even though there are numerical and physical evidences that the phase equilibrium may entail a relaxation time to reach an

**Algorithm 1** Sequential Fully Implicit Compositional Simulation Method.

---

```

1: The initial conditions:  $T, \{p_i^0\}, \{S_{\alpha,i}^0\}$  and physical rock and fluid properties
2: Specify well operation conditions ( $q_j$ )
3:  $t = 0$ 
4:  $p = p^0, S = S^0$ 
5: while  $t < t_{end}$  do
6:    $v = 1$ 
7:   while ( $\max(|\delta p^v|, |\delta s^v|) > \epsilon$  and  $v \leq v^{max}$ ) do
8:      $v_p = 1$ 
9:      $p^{v_p} = p^v$ 
10:    while ( $|\delta p^{v_p}| > \epsilon_p$  and  $v_p \leq v_p^{max}$ ) do
11:      Linearize and solve pressure equation (21) for  $p^{v_p+1}$ 
12:       $v^p \leftarrow v^p + 1$ 
13:    end while
14:     $p^{v+1} = p^{v_p+1}$ 
15:     $v_s = 1$ 
16:    while  $|\delta s^{v_s}| > \epsilon_s$  and  $v_s \leq v_s^{max}$  do
17:      Linearize and solve the saturation equation (28) for  $S^{v_s+1}$ 
18:       $v_s \leftarrow v_s + 1$ 
19:    end while
20:     $S^{v+1} = S^{v_s+1}$ 
21:    Solve component balance equation (36) obtaining  $x_c^{v+1}, y_c^{v+1}, z_c^{v+1}$ 
22:    Solve phase equilibrium equation (3), separately in each cell, to obtain  $x_c^{\bullet,v+1}, y_c^{\bullet,v+1}, z_c^{\bullet,v+1}$ 
23:    Determine saturations from phase equilibrium,  $S^{\bullet,v+1}$ 
24:    Calculate thermodynamic fluxes and update  $S^{\bullet,v+1}$ 
25:     $S^{v+1} = S^{\bullet,v+1}$ 
26:     $v \leftarrow v + 1$ 
27:  end while
28:   $t \leftarrow t + \delta t$ 
29: end while

```

---

equilibrium and the complete mixing in a grid block is not assured [37,36,10]. In comparison, the multiphase Darcy's equation is essentially linear with strongly nonlinear physical parameters (e.g., relative permeability and capillary pressure). Furthermore, the equation of state (EoS) is described by mass (molar) balance, whereas Darcy's law is based on volume balance with pore volume constraints. It is thus instructive to examine the mathematical structure of the coupled equations from two distinctly different physical systems.

Trangenstein and Bell [39] analyzed the mathematical structure of sequential compositional reservoir simulation. The pressure equation is parabolic, while the transport equation is hyperbolic. They framed the phase equilibrium computation as a constraint minimization problem of Gibbs free energy. The partial molar derivatives of fluid compressibility are employed in the analysis. They also noted the phase equilibrium cannot be strictly satisfied in a sequential algorithm. The phase equilibrium calculation provides the molar distribution among phases and the phase densities. The saturations, computed from the phase densities, do not satisfy the volume constraint. This can cause a severe numerical instability issue in compositional simulation because Darcy's equation requires that the volume constraint ( $\sum S_{\alpha} = 1$ ) is satisfied. It is quite possible that for a given time step size, there may not exist a feasible solution that strictly satisfies both Darcy's transport equation and the phase equilibrium equation. Even fully implicit schemes often encounter numerical instability, especially in phase transition. To circumvent this numerical difficulty, a different phase equilibrium calculation can be adapted (e.g. constant volume and temperature, VT-flash [25]). This new phase equilibrium includes thermodynamic pressure that is different from dynamic pressure in the transport equation. This paper proposes a new degree of freedom, "thermodynamic flux" to strictly honor the volume constraint and equalize thermodynamic and dynamic pressures.

If the phase equilibrium only redistributes the molecular components among phases, an efficient, stable sequential algorithm can be easily designed. Note that all the molecular components in a phase move with the same phase velocity. As a result, a transport equation for each component is not needed. The conventional natural variable description is followed for transport so that pressure and saturations can be solved sequentially. Since molecular components are secondary variables, the phase composition can be subsequently updated. With the updated composition, a phase equilibrium calculation is applied to compute new saturations and compositions. If the volume constraint is not violated during the phase equilibrium computation, the sequential algorithm will converge efficiently.

## 6. Algorithm summary

A sequential algorithm for pressure, saturation, and phase equilibrium calculations is summarized in Algorithm 1. All the four major steps of computation are sequentially calculated:

1. Nonlinear pressure equation, Eq. (21), is solved iteratively.
2. Nonlinear saturation equation, Eq. (28), is solved iteratively.
3. Linear component balance equation, Eq. (36), is solved.

**Algorithm 2** Potential Reordering for the Saturation and Phase Equilibrium Coupling.

---

```

1: Compute permutation matrix  $P$ , which reorders the equations based on upwind directions [16].
2:  $\nu_s = 1$ 
3: while  $|\delta s^{\nu_s}| > \epsilon_s$  and  $\nu_s \leq \nu_s^{\max}$  do
4:   Linearize and solve the permuted saturation equation (53) for  $S^{\nu_s}$ 
5:   Solve component balance equation (36) for  $x_c^{\nu_s}, y_c^{\nu_s}, z_c^{\nu_s}$ 
6:   Solve phase equilibrium equation (3), in each cell separately, to obtain  $x_c^{\bullet, \nu_s}, y_c^{\bullet, \nu_s}, z_c^{\bullet, \nu_s}$ 
7:   Determine saturations from phase equilibrium,  $S^{\bullet, \nu_s}$ 
8:    $S^{\nu_s+1} \leftarrow S^{\bullet, \nu_s}$ 
9:    $\nu_s \leftarrow \nu_s + 1$ 
10: end while

```

---

4. Phase equilibrium is computed for each cell, as described in Section 3.
5. The outer loop, comprising the stages described in steps 1 - 4, is iterated until converged.

In a practical reservoir model, the phase equilibrium calculation is limited to the three-phase region and phase transition cells. These cells can be easily identified because the pressure field is changing smoothly from the injection well to the production well. An efficient compositional reservoir simulator employs robust heuristic rules to skip unnecessary phase equilibrium computation for most part of the reservoir model, thus achieving high numerical efficiency.

In a model with phase transition around wells, Algorithm 1 is dispersive because the saturation equation moves the fluid before the phase equilibrium computation takes place. If a phase change happens in the upwind direction during the phase equilibrium computation, the downstream solution results in large dispersive errors in phase equilibrium and components balance, due to erroneous upwinding.

By replacing steps 16 - 24 in Algorithm 1 with those described in Algorithm 2, a new SFI scheme is obtained, which eliminates these numerical errors. It employs a potential reordering scheme in the saturation equation that exploits its hyperbolic nature, i.e., the cell saturation is only dependent on the cell properties in the upwind direction. As this algorithm is serial in nature, it can be expensive in modern computer architecture that utilizes memory access efficiency and parallel/vectorized computation. To overcome this, Algorithm 2 can be adaptively applied only at the first iteration in the time step and then restricted to the cells in phase transition.

## 7. Numerical examples

In this section, the convergence and accuracy of the new sequential algorithm, described in section 6, are numerically investigated. To make the examples numerically challenging, despite their simple geometries, models with large volume changes in phase equilibrium are chosen. In the first case, the primary depletion of a three-component hydrocarbon system is studied, which involves a large volume increase as the fluid pressure goes below the bubble point. The second case involves gas injection for miscible flooding [15] in a six hydrocarbon system. When the injection gas is in contact with light oil, it dissolves, causing the total fluid volume to decrease during phase transition.

With the first case, we examine the phase equilibrium characteristics in constant composition expansion, and then primary depletion is investigated with a very simple one-cell model, as well as a one-dimensional ten-cell model with one injection and one production is studied. With the second case we closely study phase transition with one cell and four-cell models. In addition, a two-dimensional model ( $10 \times 10$ ) with one injection well and one production well, located at the corners, is investigated. The latter is studied both with and without gravity effects.

### 7.1. Example 1 - a one-cell model with primary depletion

The first numerical example consists of a one-cell model perforated by a production well. Even though the model is very simple, it includes a fast phase transition that can be numerically challenging for compositional simulation. The initial fluid in the cell is composed of three hydrocarbon components and water. The initial saturations are given by  $S_w = 0.1$ ,  $S_o = 0.9$  and  $S_g = 0$  at  $T = 176^\circ\text{F}$  and  $p = 1000$  psia. The oil molar compositions are  $C_1H_4 = 0.2$ ,  $C_3H_8 = 0.3$  and  $nC_{10}H_{22} = 0.5$ . The model dimension is  $10m \times 10m \times 1m$  in physical space and the cell porosity is 0.2. A constant time-step of  $\Delta t = 0.1$  day is employed.

#### 7.1.1. Constant composition expansion

As the cell pressure decreases very rapidly during primary depletion, it is instructive to examine the phase behavior of the three-component hydrocarbon system, while disregarding the water component, in constant composition expansion [44]. The phase equilibrium state of gas and oil volumes and component compositions are plotted in Fig. 1. Above the bubble point pressure, 874.9 psia, the fluid is in single phase and the liquid has a small, positive compressibility. However, the fluid goes through a drastic total volume increase as gas evolves from the fluid below the bubble point pressure, as clearly shown in Fig. 1. Since the heavy component,  $nC_{10}H_{22}$ , does not vaporize, the gas phase is mostly composed of the lighter components, methane and propane. Note that the liquid volume becomes smaller as pressure decreases, but the specific gravity increases, because the lighter components move from the liquid phase to the gas phase. This complex

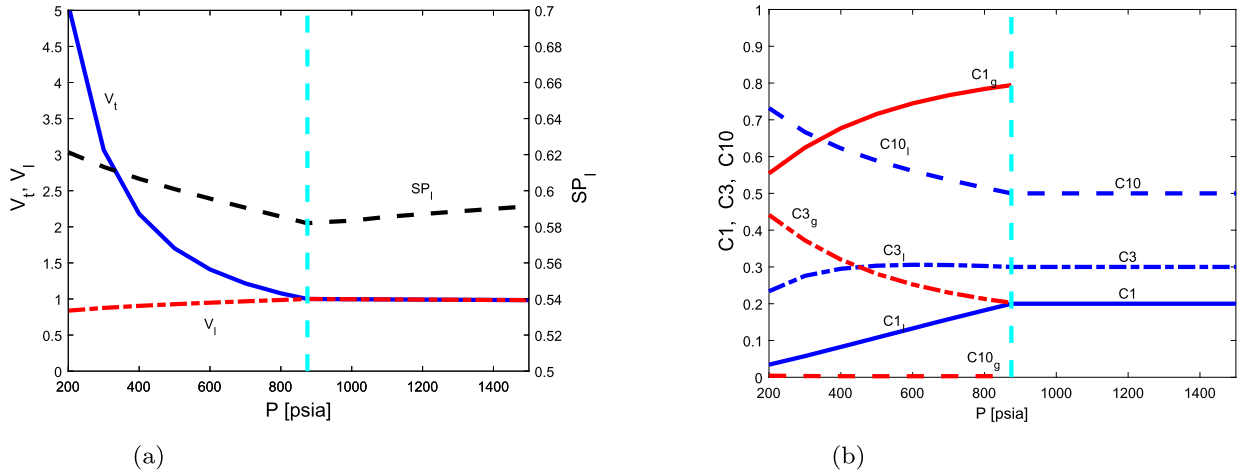


**Fig. 1.** Example 1. Phase behavior of a three-component system ( $C_1H_4 = 0.2$ ,  $C_3H_8 = 0.3$  and  $nC_{10}H_{22} = 0.5$ ) in constant composition expansion at  $T = 176^\circ\text{F}$ : (a) volume change, (b) composition distribution in gas (red) and oil (blue). (For interpretation of the colors in the figure(s), the reader is referred to the web version of this article.)

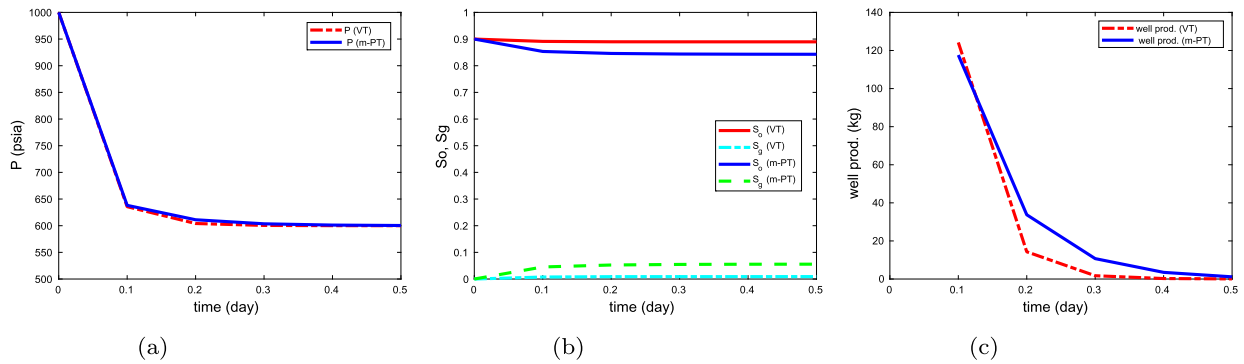


**Fig. 2.** Example 1. A single cell model with initial saturations,  $S_w = 0.1$ ,  $S_o = 0.9$  and  $S_g = 0$ .  $p_0 = 1000$  psia and  $p_{well} = 600$  psia. The primary depletion process is modeled by VT-Flash and modified PT-Flash. (a) cell pressure, (b)  $S_o$  and  $S_g$ , (c) well production rate.

phase behavior around the bubble point may cause numerical difficulties in compositional simulation that involves phase transitions.

### 7.1.2. Primary depletion

The sequential algorithm was first applied with  $\Delta t = 0.1$  day and the conventional PT-Flash. At the first outer-loop iteration, the simulation run yielded  $p = 634$  psia,  $S_w = 0.101257$ ,  $S_o = 0.85229$ , and  $S_g = 0.3389$ . Clearly the volume constraint was not satisfied due to the phase transition of hydrocarbons from single phase (oil) to two phase (oil and gas). In order to honor the multi-phase Darcy's equation, the hydrocarbon saturations were linearly normalized to  $S_o = 0.643026$  and  $S_g = 0.2557$ . We observed it creates a large mass error (20.85%) in linearly normalized saturations and the mass errors did not decrease over subsequent iterations. The algorithm failed to converge. These results are very different from those from volume constrained methods or the thermodynamic flux method. The approximation of phase behavior can yield drastic different results for the initial depletion with a large pressure drop and phase transition with a large volume change.

The same problem was simulated using the sequential algorithm with VT-flash and Modified PT-flash. As mass and volume were conserved in both methods, they yielded stable convergence by 1-3 outer loop iterations. In Figs. 2 (a) (b) and (c) the cell pressure, oil and gas saturations, and well production rates are plotted for the first 5 time steps, respectively. The pressure solutions are very similar, but the saturations show noticeable discrepancies between different phase flash approximations. The initial well rates agree in the first time step, but the subsequent declining rates are different in the second and third time steps.

The depletion process was also modeled using the thermodynamic flux, described in section 3.4. The pressure, saturations and well production with thermodynamic flux are plotted in Fig. 3. Their developments are similar to the results from VT-flash and modified PT-flash. However, the physical properties of fluids from the VT-flash and modified PT-flash are not in thermodynamic equilibrium. Note that the volume is modified to honor the volume constraint. The well production rates from the thermodynamic flux method, as a result, are very different from those from the other two methods. An accurate

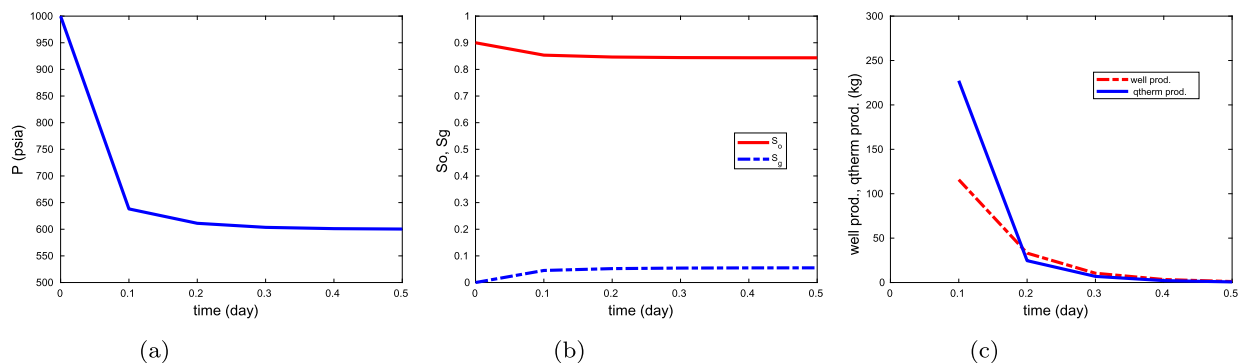


Fig. 3. Example 1. A single cell model as described in Fig. 2. The rapid depletion is modeled by the thermodynamic flux. (a) cell pressure, (b)  $S_o$  and  $S_g$ , (c) well production rate.

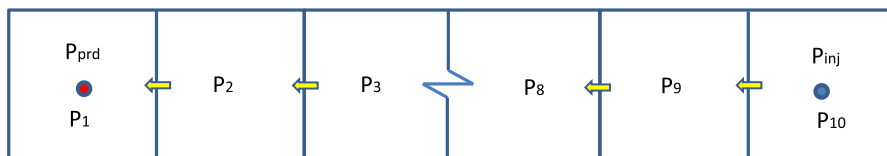


Fig. 4. Example 2: A ten-cell model with production and injection wells.

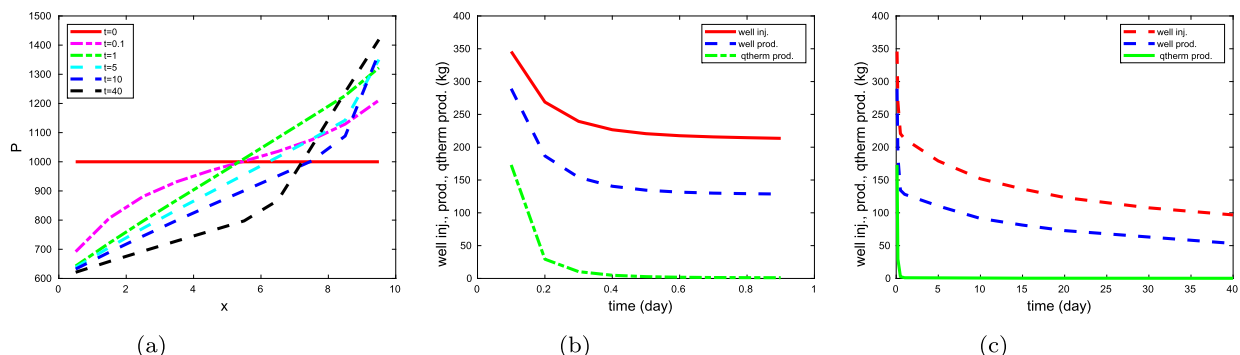


Fig. 5. Example 2. One injection well and one production well with the initial condition,  $S_w = 0.1$ ,  $S_o = 0.9$ ,  $S_g = 0$ , and  $p = 1000$  psia at  $t = 0$ . The bottom-hole pressures at the injection and production wells are given by 1400 psia and 600 psia, respectively. (a) pressure development, (b) injection rate, production rate and thermodynamic flux at early time, (c) injection rate, production rate and thermodynamic flux in simulation.

solution method is the one that follows the physical process with an infinitesimally small time-step size. A single phase fluid should be produced before the bubble point pressure is reached and then, the second phase should appear gradually at the production. The pore volume constraint will delay gas production. When the thermodynamic flux is added as an additional degree of freedom, the physical properties at the computed pressure and temperature can be readily honored.

This simple problem is an extreme test for phase equilibrium because of the large pressure drop ( $> 450$  psia) and phase transition in the first time step. Note that the numerical difficulty can be easily resolved if a mass/volume conservative flash approximation is applied.

### 7.2. Example 2: a ten-cell model with production and injection wells

The previous example with three-hydrocarbon components, was recast to a simple 1-d model of linear displacement. The model is schematically depicted in Fig. 4, where a water injection well is located in cell  $i = 10$  and a production well in cell  $i = 1$ . The model was initialized with  $p = 1000$  psia and the bottom hole pressures of the injection and production wells are maintained at 1400 and 600 psia, respectively. A constant time step size,  $\Delta t = 0.1$  day, is employed throughout the simulation. Despite the sudden initial change in pressure and volume, the application of thermodynamic flux renders a stable and convergent numerical solution without time step cuts. In Fig. 5 the pressure developments and the well rates and thermodynamic flux are plotted. The thermodynamic flux is needed to compensate sudden pressure change that incurs additional production of fluid at the early stages of the simulation. But in the later time, the thermodynamic flux diminishes quickly as the system enters a stable operation mode (see Fig. 5(c)).

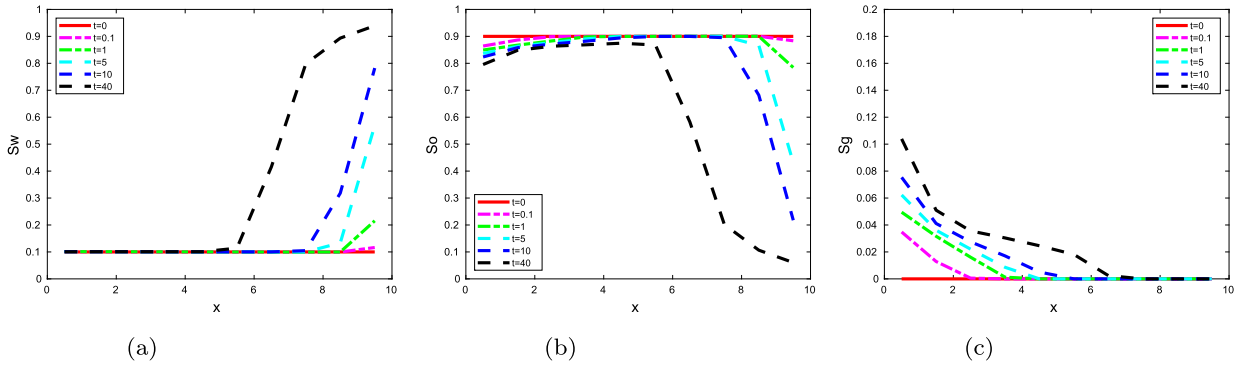


Fig. 6. Example 2. Saturation distribution. (a)  $S_w$ , (b)  $S_o$ , (c)  $S_g$ .

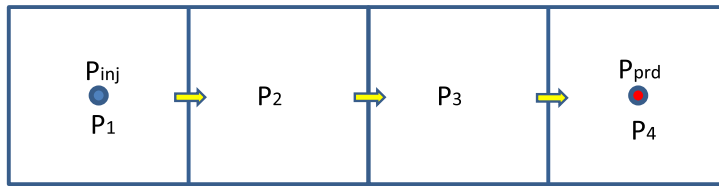


Fig. 7. Example 4. A four cell model with production and injection wells.

The uniform initial pressure quickly redistributes to honor the well constraint and the profile continuously adjusts to reflect the total mobility of fluids. Note that the viscosities of water, oil and gas are 1, 0.1695, and 0.00126 cp, respectively, at  $t = 40$  days. Fig. 5(a) clearly shows that the pressure gradient reflects the total fluid mobility as the water moves from the injection well. In Fig. 6, gas evolves as low pressure propagates from the productions well.

### 7.3. Example 3: a one-cell model with miscible gas injection

This example employs the six component hydrocarbon fluid of the SPE Fifth Comparative Solution Project [15]. The oil composition is  $C_1 = 0.50$ ,  $C_3 = 0.03$ ,  $C_6 = 0.07$ ,  $C_{10} = 0.20$ ,  $C_{15} = 0.15$ , and  $C_{20} = 0.05$ , while the injection gas composition is  $C_1 = 0.77$ ,  $C_3 = 0.20$ , and  $C_6 = 0.03$ . The detailed physical properties of fluids can be found in [15]. When oil and injection gas are in contact, they become miscible. Consequently, the total fluid volume may shrink due to phase equilibrium. It is thus instructive to examine numerical convergence of the SFI algorithm on a one-cell model with a miscible gas injector.

The cell is initialized with pressure at 2500 psia, temperature 160°F, and phase saturation  $S_w = 0.2$ ,  $S_o = 0.7999$  and  $S_g = 0.0001$ . The gas injector has a constant bottom-hole pressure 2600 psia. The cell size is  $10m \times 10m \times 1m$  and the porosity is 0.2. A constant time step size of  $\Delta t = 1$  day is employed throughout the simulation. The actual convergence path in SFI was:

1. For given initial condition and well operation constraint, the pressure calculation yields the cell pressure  $p_0 = 2599.9044$  psia and the amount of injected gas is 8.9778 kg.
2. The saturation computation yields  $S_w = 0.199347$ ,  $S_o = 0.798355$  and  $S_g = 0.002298$ . Due to the low compressibility of oil, the amount of injected gas is limited,  $q_{inj} = 8.9778$  kg, and the cell pressure approaches the well-bore pressure.
3. The phase equilibrium of hydrocarbons yields  $S_o = 0.799772$  and  $S_g = 0$ . The gas phase disappears and the volume constraint is not satisfied ( $S_w + S_o + S_g \neq 1$ ).
4. The thermodynamic flux is computed to satisfy the volume constraint:  $q_{therm} = 5.81615$  kg.
5. The second iteration brings  $p_0 = 2599.84556$  psia and  $q_{inj} = 14.7886$  kg, which satisfy the mass and volume conservation of the governing equations.

In this example the new algorithm efficiently yields a consistent solution that satisfies both mass and volume constraints. In sequential compositional simulation, the large fluid volume variation in phase transition has been numerically challenging. Inclusion of the thermodynamic flux significantly improves numerical convergence for this challenging problem.

### 7.4. Example 4: a four-cell model with miscible-gas injection and production wells

A four cell-model with injection and production wells with the same SPE 5 fluid model which was used in the previous example, is studied. The four-cell model is schematically depicted in Fig. 7. It was initialized with  $p = 2500$  psia and  $T = 160^\circ\text{F}$ .

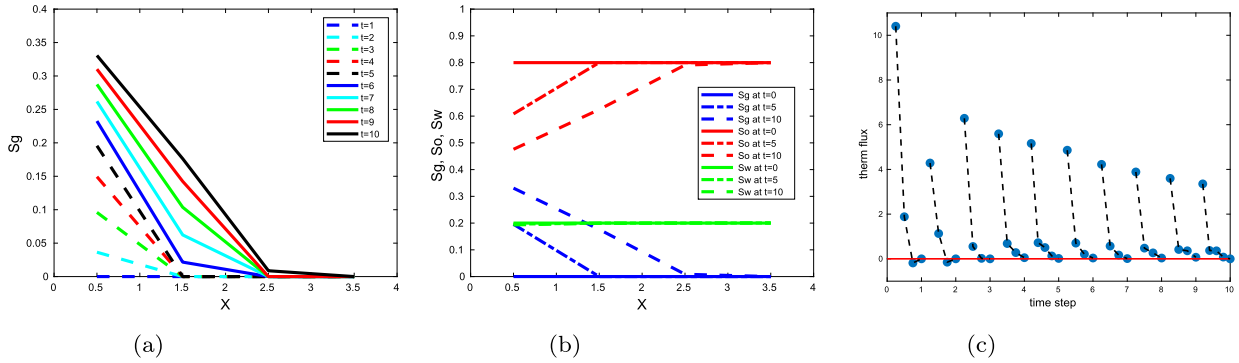


**Fig. 8.** Example 4. A four-cell model with injection and production wells with the initial condition,  $S_w = 0.2$ ,  $S_o = 0.7999$ ,  $S_g = 0.0001$ , and  $p = 2500$  psia at  $t = 0$ . The bottom-hole pressures at the injection and production wells are given by 2600 psia and 2400 psia, respectively: (a) gas saturation development, (b) saturation distribution, (c) thermodynamic flux at cell 1 during nonlinear iterations of the outer loop.

As discussed in the previous numerical example, the injection gas is dissolved in oil on first contact. The phase transition incurs a large volume change. If the saturation equation is solved for all the cells before phase equilibrium calculation, the injection gas invades several cells. This will create unnecessary numerical dispersion. In order to control the error, the saturation and phase equilibrium of the injection cell are first solved to provide a better estimate of saturations and composition. This can be considered as a potential-based reduced Newton algorithm for saturation equation [17]. This potential-based Newton algorithm (see Algorithm 2 in section 6) is needed for the cells with large changes of cell properties (e.g., saturations and compositions). Algorithm 2 is, thus, employed for the first iteration of the saturation solution loop.

The model is simulated for 10 days with a fixed 1 day time-step size. Convergence is typically achieved after 3-5 outer-loop iterations. The saturation profiles and the thermodynamic flux are depicted over the course of simulation time in Figs. 8 (a), (b) and (c). Note that at the first time step, all the injection gas was dissolved into oil and the fluid volume was smaller than the pore volume. A thermodynamic flux of injection gas is introduced to satisfy the volume constraint, as shown in Fig. 8 (c). In Fig. 8 (a), the gas saturation in cell 1 builds up gradually, despite the fact that part of the injected gas is continuously dissolved into oil. Note that the water saturation hardly changes over the simulation. The thermodynamic flux is non-monotonic at the initial time step (1-3), but monotonically decreases afterwards.

### 7.5. Example 5. A 2-d model with miscible-gas injection well and production wells

A 2-dimensional model is considered to investigate the gravitational effect in multi-phase, compositional flow. The physical dimension of the model is  $100m \times 100m \times 1m$  that is uniformly discretized over  $10 \times 10 \times 1$  grids. As in Examples 3 and 4, the 6-component hydrocarbon fluid from the SPE Fifth Comparative Solution Project [15] is employed. The model is initialized with  $S_o = 1$  at  $p = 2500$  psia and  $T = 160^\circ\text{F}$ . The wells are located at the corners of the domain with constant pressure constraints: the injection well at (1, 1) with  $p_{well}^{inj} = 2600$  psia and the production well at (10, 10) with  $p_{well}^{prd} = 2400$  psia. To examine multi-phase flow interactions with phase equilibrium and gravity effect, the water phase is not included in this example.

The model is first simulated without gravity and the results are shown in Fig. 9: (a)  $p$  at  $t=100$  days, (b)  $S_g$  at 100 days, and (c)  $S_g$  at 400 days. Note that the diagonal symmetry of the solution is strictly honored during the simulation. The results with gravity are shown in Fig. 10. The pressure and gas saturation distribution in the presence of gravity are very different from those without gravity. As the injected gas interacts with oil, the system becomes two phase. The gas phase moves preferentially in vertical direction due to buoyancy. Furthermore, it is noted that the gas injection and production rates between these two scenarios are very different due to the different potential differences at the well location with or without gravity. The density and viscosity of the gas phase are much smaller than those of oil phase. Consequently, the buoyancy effect is very visible in Figs. 10 (b) and (c), as the gas phase moves in the vertical direction away from the injection well.

In the early stages of simulation, the phase behavior is complex around the well as the gas phase becomes miscible with oil. Since Algorithm 2 is numerically more expensive than Algorithm 1, it is, thus, applied only for the injection cell (1, 1) and two downstream cells (2, 1) and (1, 2). The thermodynamic flux efficiently stabilizes the numerical calculation, allowing a fixed time step of 1 day throughout simulation. For this numerical example, the new algorithm takes 4-6 outer-loop iterations at each time step before achieving convergence.

## 8. Concluding remarks

General purpose reservoir simulators commonly adapt the compositional formulation because it can model complex physical processes. In addition, the black-oil formulation can be included as a simplified form of the compositional formu-

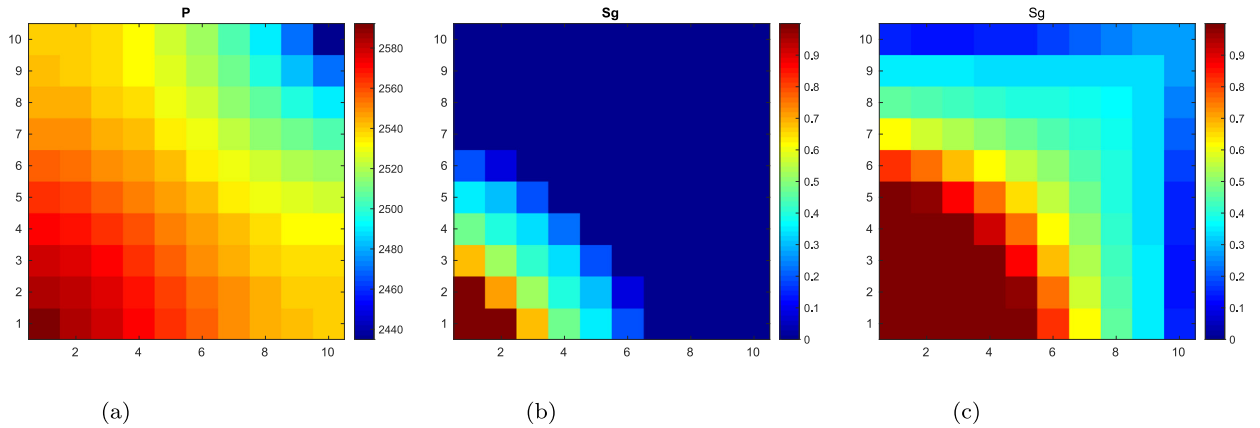


**Fig. 9.** Example 5. A 2-d model with no gravity effect: initial saturations are given by  $S_o = 1$  and  $S_w = S_g = 0.0$ .  $p_0 = 2500$  psia, at  $t = 0$ , and the well pressures are specified by  $p_{well}^{inj} = 2600$  psia, and  $p_{well}^{prd} = 2400$  psia. (a)  $p$  at  $t = 100$  days, (b)  $S_g$  at  $t = 100$  days and (c)  $S_g$  at  $t = 400$  days.

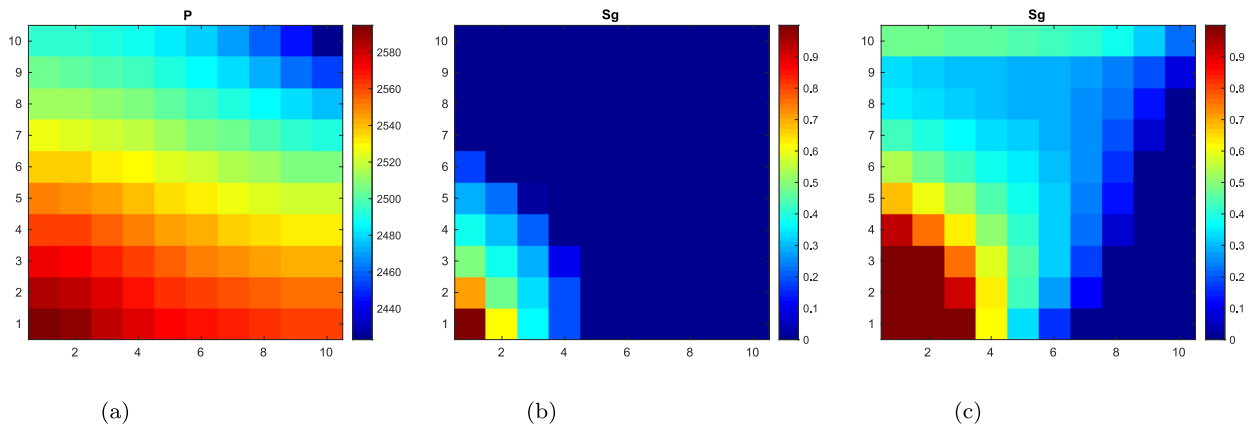


**Fig. 10.** Example 5. A 2-d model with gravity: the initial and operational conditions are given in the caption of Fig. 9: (a)  $p$  at  $t = 100$  days, (b)  $S_g$  at  $t = 100$  days, and (c)  $S_g$  at  $t = 400$  days.

lation. In general, the time scale for phase equilibrium is assumed to be much smaller than the characteristic time of the transport process. The phase equilibrium is computed by the Equation of State (EoS), e.g., Peng-Robinson.

In this paper, observing that components within a phase are displaced with the same velocity at grid cell interfaces, we formulate simplified governing equations for compositional flow that are similarly structured to those from the black-oil formulation. Since the characteristics of the transport equations and the EoS are distinctly different, a sequential algorithm is designed, which separates each process to be tackled by dedicated solution methods. Nonetheless, it has been a real challenge to develop a robust and efficient sequential algorithm, which, in contrast to previously published work, would strictly satisfy all the governing equations, i.e., mass and volume conservations and phase equilibrium [28]. If the fluid goes through a phase transition that involves a large volume change, the sequential algorithm needs many iterations or fails to converge. This indicates that the governing equation may not capture the significant volume change associated with the phase transition. Based on this observation, a new sequential algorithm was devised, which includes a new degree of freedom, “thermodynamic flux”, to represent the phase equilibrium in a confined space.

Two versions of the Sequential Fully Implicit Method for compositional simulation are proposed:

1. In the first algorithm, all the processes are divided into four steps, to be solved in sequence: pressure, saturation, components, and phase equilibrium.
2. The second algorithm reorders the cells based on upwind direction, and saturation, component and phase equilibrium for each cell are solved in sequence, in serial manner.

Clearly Algorithm 2 can be expensive in modern hardware, that exploits parallel and vector computation. It is, thus, used only for cells which experience phase transition at the first iteration of the time step. This ensures numerical stability while minimizing numerical dispersion during the computation of the saturation and phase equilibrium.

The new algorithm was demonstrated on two numerically challenging problems with phase transition accompanied by fluid volume changes: (1) rapid primary depletion and (2) miscible gas injection. The first case involved a large volume increase, while the second case featured a fluid volume decrease as gas dissolves on contact with oil. The new algorithm successfully resolved these challenging phase flow problems. The method was also employed on a 2-dimensional, miscible flooding example with and without gravity.

The numerical examples show that the conventional compositional formulation with instantaneous phase equilibrium is incomplete in describing the phase transition with a large volume change. This is identified as the prime cause for convergence failure during phase transition, experienced using state-of-the-art sequential methods. Finally, the inclusion of the thermodynamic flux was shown to accelerate the convergence of the nonlinear iterative scheme.

In future work, the efficiency of the new algorithm in more complex physical models with compressibility, gravity, capillary force and three-phase flow, needs to be demonstrated. In addition, the direct applicability of the method to black-oil models needs to be demonstrated. Finally, the convergence path of a fully implicit method during a phase transition is to be studied and compared with that of the proposed algorithm. Most commercial compositional simulators often adapt rescaling or chopping of variables that lie outside of the physical boundary. The mathematical implications of such ad-hoc treatments in highly nonlinear problems need to be closely examined.

### CRediT authorship contribution statement

**S.H. Lee:** Conceptualization, Formal analysis, Writing - original draft. **M. Tene:** Formal analysis, Software, Writing - review & editing. **S. Du:** Software. **X. Wen:** Funding acquisition, Supervision, Writing - review & editing. **Y. Efendiev:** Conceptualization, Formal analysis, Writing - review & editing.

### Declaration of competing interest

The authors declare that they have no known competing financial interests or personal relationships that could have appeared to influence the work reported in this paper.

### Acknowledgements

This work was supported by Chevron/Schlumberger Intersect Alliance Technology.

### References

- [1] G. Ács, S. Doleshall, S. Fakas, General purpose compositional model, *Soc. Pet. Eng. J.* (1985) 543–553.
- [2] Y. Brenier, J. Jaffre, Upstream differencing for multiphase flow in reservoir simulation, *SIAM J. Numer. Anal.* 28 (1991) 685–696.
- [3] M.C.H. Chien, S.T. Lee, W.H. Chen, A new fully implicit compositional simulator, in: *Proceedings of 7th SPE Symposium on Reservoir Simulation: SPE 12244*, San Francisco, CA, 1983, pp. 113–122.
- [4] K.H. Coats, Reservoir simulation: state of the art, *J. Pet. Technol.* (1982) 1633–1642.
- [5] L.D. Gelb, K.E. Gubbins, R. Radhakrishnan, M. Sliwinski-Bartkowiak, Phase separation in confined systems, *Rep. Prog. Phys.* 62 (1999) 1573–1659.
- [6] H. Hajibeygi, H.A. Tchelepi, Compositional multiscale finite volume formulation, *SPE J.* 19 (2012) 316–326.
- [7] F.P. Hamon, B.T. Mallison, H.A. Tchelepi, Implicit hybrid upwinding for coupled multiphase flow and transport with gravity, *Comput. Methods Appl. Mech. Eng.* 311 (2016) 599–624.
- [8] F.P. Hamon, B.T. Mallison, H.A. Tchelepi, Hybrid upwinding for two phase flow in heterogeneous porous media with gravity and capillarity, in: *Proceedings of ECMOR 15, Th Efe08*, Amsterdam, Netherlands, August 29 – September 1, 2016.
- [9] F.P. Hamon, H.A. Tchelepi, Analysis of hybrid upwinding for fully-implicit simulation of three-phase flow with gravity, *SIAM J. Numer. Anal.* 54 (2016) 1682–1712.
- [10] I.M. Indrupskiy, O.A. Lobanova, V.R. Zubov, Non-equilibrium phase behavior for hydrocarbons in compositional simulation and upscaling, *Comput. Geosci.* 21 (2017) 1173–1188.
- [11] P. Jenny, S.H. Lee, H.A. Tchelepi, Multi-scale finite-volume method for elliptic problems in subsurface flow simulation, *J. Comput. Phys.* 187 (2003) 47–67.
- [12] P. Jenny, S.H. Lee, H.A. Tchelepi, Adaptive multiscale finite volume method for multi-phase flow and transport, *Multiscale Model. Simul.* 3 (2004) 50–64.
- [13] P. Jenny, H.A. Tchelepi, S.H. Lee, Unconditionally convergent nonlinear solver for hyperbolic conservation laws with s-shaped flux functions, *J. Comput. Phys.* 228 (2009) 7497–7512.
- [14] P. Jenny, C. Wolfsteiner, S.H. Lee, L.J. Durlofsky, Modeling flow in geometrically complex reservoirs using hexahedral multi-block grids, in: *Proceedings of 16th SPE Symposium on Reservoir Simulation, SPE Paper 66357*, Houston, TX, 2001.
- [15] J.E. Killough, C.A. Kossack, Fifth comparative solution project: evaluation of miscible fluid simulator, in: *Proceedings of 9th SPE Symposium on Reservoir Simulation: SPE 16000*, San Antonio, TX, 1987.
- [16] Ø.S. Klemetsdal, A.F. Rasmussen, O. Møyner, K.-A. Lie, Efficient reordered nonlinear Gauss-Seidel solvers with high order black-oil models, in: *Proceedings of ECMOR 16, Mo A2 10*, Barcelona, Spain, September 3–6, 2018.
- [17] F. Kwok, H.A. Tchelepi, Potential-based reduced Newton algorithm for nonlinear multiphase flow in porous media, *J. Comput. Phys.* 227 (2007) 706–727.
- [18] S.H. Lee, Y. Efendiev,  $C^1$ -continuous relative permeabilities and hybrid discretization for three-phase flow in porous media, *Adv. Water Resour.* 96 (2016) 209–224.
- [19] S.H. Lee, Y. Efendiev, Hybrid discretization of multi-phase flow in porous media in the presence of viscous, gravitational and capillary forces, *Comput. Geosci.* 22 (2018) 1403–1421.
- [20] S.H. Lee, Y. Efendiev, H.A. Tchelepi, Hybrid upwind discretization of nonlinear two-phase flow with gravity, *Adv. Water Resour.* 82 (2015) 27–38.
- [21] S.H. Lee, C. Wolfsteiner, H.A. Tchelepi, A multiscale finite-volume method for multiphase flow in porous media: black oil formulation of compressible, three phase flow with gravity and capillary force, *Comput. Geosci.* 12 (2007) 351–366.

- [22] I. Lunati, M. Tyagi, S.H. Lee, An iterative multiscale finite volume algorithm converging to exact solution, *J. Comput. Phys.* 230 (2011) 1849–1864.
- [23] M.L. Michelsen, The isothermal flash problem. Part I. Stability, *Fluid Phase Equilib.* 9 (1982) 1–19.
- [24] M.L. Michelsen, The isothermal flash problem. Part II. Phase split calculation, *Fluid Phase Equilib.* 9 (1982) 21–40.
- [25] M.L. Michelsen, State function based flash specification, *Fluid Phase Equilib.* 158–160 (1999) 617–626.
- [26] J. Mikyška, A. Firoozabadi, A new thermodynamic function for phase-splitting at constant temperature, moles and volume, *AIChE J.* 57 (2011) 1897–1904.
- [27] A. Moncorgé, H.A. Tchelepi, P. Jenny, Modified sequential fully implicit scheme for compositional flow simulation, *J. Comput. Phys.* 337 (2017) 98–115.
- [28] A. Moncorgé, H.A. Tchelepi, P. Jenny, Sequential fully implicit formulation for compositional simulation using natural variables, *J. Comput. Phys.* 371 (2018) 690–711.
- [29] O. Møyner, A. Moncorgé, Nonlinear domain decomposition scheme for sequential implicit formulation of compositional multiphase flow, in: *Proceedings of ECMOR XVI, Mo A2 08, Barcelona, Spain, 2018.*
- [30] O. Møyner, H.A. Tchelepi, A mass-conservative sequential implicit multiscale method for isothermal equation-of-state compositional problems, *SPE J.* 23 (2018) 2376–2393.
- [31] L.X. Nghiem, P.H. Sammon, A non-equilibrium equation of state compositional simulator, in: *Proceedings of the 1997 SPE Reservoir Simulation Symposium: SPE 37980, Dallas, TX, 1997, pp. 65–69.*
- [32] J.S. Nolen, D.W. Berry, Test of the stability and time-step sensitivity of semi-implicit reservoir simulation techniques, *Soc. Pet. Eng. J.* (1972) 253–266.
- [33] H. Pan, H.A. Tchelepi, Reduced-variables method for general purpose compositional reservoir simulation, spe 131737, in: *Proceedings of the CPS/SPE International Oil and Gas Conferences, Beijing, China, 2010.*
- [34] D.Y. Peng, D.B. Robinson, A new two-constant equation of state, *Chem. Eng. Sci.* 27 (1972) 1197–1340.
- [35] D.Y. Peng, D.B. Robinson, A new two-constant equation of state, *Chem. Eng. Fundam.* 15 (1976) 59–64.
- [36] A. Salehi, D.V. Voskov, H.A. Tchelepi, Thermodynamically consistent transport coefficients for upscaling of compositional processes, in: *Proceedings of the 2013 SPE Reservoir Simulation Symposium: SPE 163576, The Woodlands, TX, 2013.*
- [37] M.R. Todd, W.J. Longstaff, The development, testing, and application of a numerical simulator for predicting miscible flood performance, *Proc. AIME* 253 (1972) 874–882.
- [38] J.A. Trangenstein, J.B. Bell, Mathematical structure of black-oil reservoir simulation, *SIAM J. Appl. Math.* 49 (1989) 749–783.
- [39] J.A. Trangenstein, J.B. Bell, Mathematical structure of compositional reservoir simulation, *SIAM J. Sci. Stat. Comput.* 10 (1989) 817–845.
- [40] D. Voskov, An extended natural variable formulation for compositional simulation based on tie-line parameterization, *Transp. Porous Media* 92 (2012) 541–557.
- [41] D. Voskov, H.A. Tchelepi, Comparison of nonlinear formulation for two-phase multi-component EoS based simulation, *J. Pet. Sci. Eng.* (2012) 101–111.
- [42] X. Wang, H.A. Tchelepi, Trust-region based solver for nonlinear transport in heterogeneous porous media, *J. Comput. Phys.* 253 (2013) 114–137.
- [43] J.W. Watts, A compositional formulation of the pressure and saturation equations, *SPE Reserv. Eng.* (1986) 243–252.
- [44] C.H. Whitson, M.R. Brulé, *Phase Behavior, SPE Monograph, vol. 20, Soc. of Pet. Eng., Dallas, Texas, 2000.*
- [45] L.C. Young, R.E. Stephenson, A generalized compositional approach for reservoir simulation, *Soc. Pet. Eng. J.* (1983) 727–742.
- [46] R. Younis, H.A. Tchelepi, K. Aziz, Adaptively localized continuation Newton: nonlinear solvers that converges all the time, *SPE J.* (2010) 526–544.